High-Temperature Materials

SCIEPublish

Article

Microstructural Evolution and Mechanical Properties of Post-Processed IN 625 Fabricated by Laser Powder Bed Fusion

Alber Sadek *

Edison Welding Institute (EWI), Columbus, OH 43221, USA

* Corresponding author. E-mail: asadek@ewi.org (A.S.)

Received: 6 December 2025; Revised: 10 March 2026; Accepted: 13 April 2026; Available online: 24 April 2026

ABSTRACT: Laser powder bed fusion (LPBF) is widely used for manufacturing nickel-based superalloy components with complex geometries; however, the process produces non-equilibrium microstructures characterized by directional grain growth, cellular substructures, and compositional segregation, which can lead to anisotropic mechanical behavior. In this study, the influence of multiple post-processing heat-treatment routes on the microstructural evolution and mechanical properties of LPBF-fabricated Inconel 625 (IN625) was systematically investigated by combining stress relief, hot isostatic pressing (HIP), and solution annealing. Microstructural characterization was performed using optical microscopy and scanning electron microscopy, while tensile properties were evaluated from room temperature to 700 °C. The HT3 condition resulted in a fully recrystallized, equiaxed grain structure with reduced segregation and minimal Nb-rich Laves phase, leading to nearly isotropic mechanical properties, with an ultimate tensile strength of approximately 880 MPa and an elongation exceeding 50%. Elevated-temperature testing demonstrated stable mechanical performance, with a localized strengthening effect near 600 °C attributed to dynamic strain aging. These results demonstrate that appropriate post-processing can effectively homogenize LPBF IN625 and improve its mechanical reliability.

Keywords: Inconel 625; Laser powder bed fusion; Additive manufacturing; Heat treatment; Microstructure; Mechanical properties

1. Introduction

Additive manufacturing has progressed from a prototyping approach to a viable method for producing load-bearing metallic components with complex geometries and reduced material waste. Among the available techniques, laser powder bed fusion (LPBF) has gained widespread adoption because it enables localized melting and solidification of powder layers to generate near-net-shape parts directly from digital models [1–5]. This capability has expanded its use in applications where conventional manufacturing routes are either inefficient or impractical.

Nickel-based superalloys are frequently processed using LPBF due to their ability to retain mechanical strength and resist degradation under demanding thermal and chemical environments. Inconel 625 (IN625), a solid-solution-strengthened nickel–chromium alloy, is widely used in aerospace, marine, and energy

systems due to its resistance to corrosion, oxidation, and high-temperature deformation [6–9]. The distribution and interaction of alloying elements such as niobium and molybdenum within the matrix strongly influence its mechanical performance.

The thermal conditions associated with LPBF differ substantially from those in conventional processing, leading to distinct microstructural features. Rapid solidification combined with directional heat extraction promotes the formation of elongated grains aligned with the build direction. Within these grains, fine-scale cellular structures develop, accompanied by localized compositional variations [10–15]. These compositional gradients frequently result in the accumulation of niobium and molybdenum in interdendritic regions, which can lead to the formation of Nb-rich phases such as the Laves phase [16–20]. Such phases are generally associated with reduced ductility and inferior fatigue performance.

These microstructural characteristics contribute to anisotropic mechanical behavior, which limits the reliability of LPBF-fabricated components in structural applications. Heat-treatment procedures developed for wrought IN625 are not always effective in modifying the directional grain structure or eliminating segregation present in LPBF materials [21–23]. Consequently, post-processing strategies must be specifically designed to address the unique microstructural features produced during LPBF.

Thermal treatments such as stress relief, hot isostatic pressing (HIP), and solution annealing have been explored to improve the microstructural uniformity of LPBF nickel-based alloys [24–28]. These processes affect the microstructure through mechanisms such as diffusion, phase transformation, and recrystallization. Elevated-temperature treatments, in particular, can reduce segregation and dissolve Nb-rich phases, thereby enhancing ductility and mechanical stability [29–35]. However, many existing studies consider these processes individually, and the combined effects of multiple post-processing steps remain less clearly defined [36–47].

Furthermore, the effectiveness of post-processing is influenced by variables such as temperature, time, and cooling conditions, which govern grain growth, phase evolution, and the degree of anisotropy [48–52]. A systematic evaluation of these parameters in combination is therefore required to establish reliable processing–structure–property relationships.

In this study, a series of heat-treatment routes incorporating stress relief, HIP, and solution annealing are investigated to determine their influence on the evolution of microstructure and mechanical performance in LPBF-fabricated IN625. The objective is to identify processing conditions that transform the as-built microstructure into a homogeneous and recrystallized state, thereby improving mechanical consistency over a broad temperature range.

2. Materials and Methods

2.1. Materials and Additive Manufacturing Process

Gas-atomized Inconel 625 (IN625) powder was utilized as the feedstock material for all builds. The powder exhibited a particle size distribution of approximately 10–45 μm and was produced under an inert atmosphere to minimize oxidation and contamination. The nominal chemical composition of the powder is provided in Table 1.

Table 1. Chemistry of Used Powder in Weight Percent.

C	Mn	Si	Cr	Nb	Ti	Mo	Al	Ta	Fe	Ni	O	N	H
0.02	<0.01	0.04	21.34	3.43	0.05	8.87	0.03	0.01	3.10	Bal.	0.012	0.005	0.002

All coupons were fabricated using an EOS M280-400 system (EOS GmbH, Krailling, Germany) equipped with a 400 W Yb-fiber laser and operated with PSW software version 3.6.32.1. The LPBF process

was conducted in an argon atmosphere, with oxygen levels maintained between 70 and 120 ppm. The scanning direction was rotated by 60° between adjacent layers to promote microstructural homogeneity.

Based on prior parameter optimization, the selected processing conditions were a laser power of 300 W, a scan speed of 1000 mm/s, a hatch spacing of 110 μm, and a layer thickness of 40 μm. For heat-treatment trials, 15-mm cubes were fabricated directly on a stainless-steel substrate. Additionally, eight wall specimens measuring 150 × 150 × 15 mm were produced for mechanical testing.

2.2. Heat Treatment

A series of post-build thermal treatments was designed to evaluate the influence of different processing routes on the microstructural evolution of LPBF-fabricated IN625. Five distinct conditions (HT1–HT5) were established, each incorporating different combinations of thermal exposure, pressure-assisted processing, and solutionizing steps.

The applied thermal cycles included high-temperature stress-relief treatments, hot isostatic pressing (HIP), and solution annealing. The stress-relief treatment was conducted at approximately 1040 °C with a holding period of 60 min to reduce residual stresses generated during the LPBF process. HIP processing was performed at approximately 1120 °C under an applied pressure of 100 MPa for 4 h, to reduce internal porosity and promote diffusion-driven homogenization. Solution annealing treatments were carried out within the temperature range of 1175–1200 °C to facilitate dissolution of segregated phases and promote recrystallization.

Each heat-treatment route was configured to isolate the effect of specific processing sequences. The HT1 condition consisted of stress relief followed by controlled cooling, while HT2 involved HIP without prior high-temperature exposure. The HT3 condition combined stress relief with subsequent HIP processing to evaluate the interaction between thermal and pressure-assisted treatments. The HT4 and HT5 conditions incorporated higher-temperature solution annealing steps to investigate their effect on grain growth, phase dissolution, and microstructural uniformity.

Temperature selection and holding durations were based on thermodynamic considerations and prior studies on IN625, ensuring sufficient activation of diffusion processes required for homogenization and recrystallization. The variation among the selected conditions enables a systematic comparison of how different post-processing strategies influence the resulting microstructure and associated mechanical behaviour.

The detailed heat-treatment conditions investigated in this study are summarized in Table 2.

Table 2. Heat treatment procedures.

Heat Treatment	Stress Relief		HIP		Solution Anneal	
	Tempe. (°C)	Time, (min.)	Tempe. (°C)	Time, (min.)	Tempe. (°C)	Time, (min.)
HT1	1040	60			1175	60
HT2			1120	240		
HT3	1040	60	1120	240		
HT4			1120	240	1175	60
HT5					1200	30

2.3. Sample Preparation and Characterization

Specimens were sectioned from the fabricated components to enable evaluation in both the build direction (XZ plane) and the transverse direction (XY plane), allowing assessment of orientation-dependent features. All samples were mounted in conductive media to facilitate both optical and electron microscopy.

Surface preparation was carried out through a sequence of mechanical grinding and polishing steps designed to produce a deformation-free surface suitable for microstructural analysis. Grinding was performed using progressively finer abrasive media, followed by polishing with diamond suspensions of

decreasing particle size. Final surface finishing was completed using a fine colloidal silica suspension to minimize surface deformation and enhance microstructural contrast.

Chemical etching was performed using Kalling's reagent to reveal grain boundaries and microstructural features. Etching conditions were adjusted to ensure clear delineation of cellular structures, grain morphology, and secondary phases without over-etching.

Microstructural characterization was conducted using optical microscopy for general morphology and scanning electron microscopy (SEM) for higher-resolution observations. Energy-dispersive spectroscopy (EDS) was employed to determine local chemical variations and to identify compositional differences associated with segregated regions and precipitates.

Grain size measurements were performed in accordance with ASTM E112 [53] using the linear intercept approach. Multiple fields of view were analyzed for each sample to ensure representative results, and measurements were obtained along different orientations to capture potential anisotropy.

Mechanical testing specimens were prepared in accordance with ASTM E8 [54] for room-temperature testing and ASTM E21 [55] for elevated-temperature evaluation. Tensile specimens were machined from fabricated material with orientations aligned to both the build and transverse directions to assess the directional dependence of mechanical behavior.

3. Results and Discussions

3.1. As Build Microstructure

The microstructure of LPBF-fabricated IN625 in the as-built condition is characterized by a hierarchical arrangement of features that originate from the localized melting and rapid solidification inherent to the process, as shown in Figure 1. At the macroscopic scale, overlapping melt pool boundaries are clearly visible, reflecting the sequential scanning strategy and layer-wise material deposition. These boundaries exhibit a characteristic curved geometry corresponding to the thermal profile of the moving laser, and they define regions of repeated thermal cycling throughout the build.

At the grain scale, a pronounced directional morphology is observed. Grains are elongated and extend predominantly along the build direction, forming columnar structures that traverse multiple deposited layers. This morphology results from the thermal gradient established during solidification, where heat is preferentially conducted away from the melt pool into the previously solidified material. The resulting solidification front promotes epitaxial growth, allowing grains to propagate across layer boundaries without interruption. This behavior leads to a strong crystallographic texture and contributes to anisotropic mechanical properties.

Within these columnar grains, a fine cellular substructure is present. The cellular features are defined by compositional fluctuations that develop during rapid solidification, where solute redistribution occurs on a microscale. The cell boundaries correspond to regions of solute enrichment, while the cell interiors remain relatively depleted. Energy-dispersive spectroscopy (EDS) analysis confirms that niobium and molybdenum are concentrated along these boundaries, indicating segregation of alloying elements during the final stages of solidification.

The enrichment of niobium in interdendritic regions promotes the formation of Nb-rich secondary phases, commonly identified as the Laves phase. These phases result from non-equilibrium solidification conditions and are typically located along cellular boundaries and within interdendritic networks. Due to their brittle nature, such phases can act as preferential sites for crack initiation under mechanical loading and are therefore considered detrimental to ductility and fatigue performance.

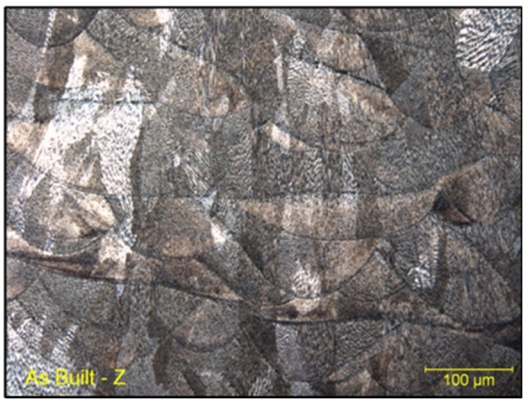

XZ-Plane XY-Plane

Optical Images of the As-built Microstructure

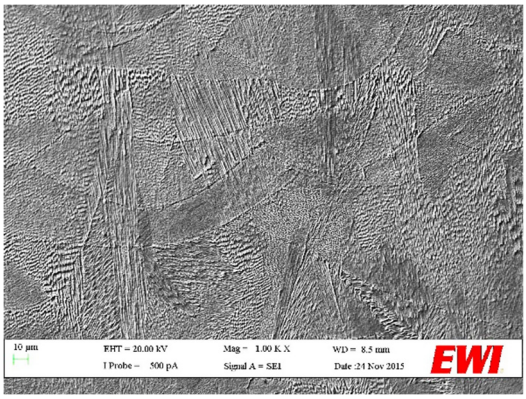

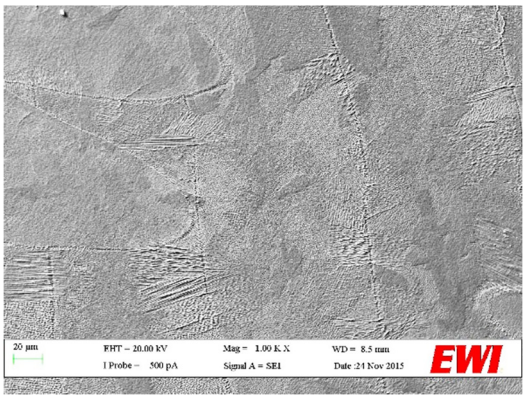

XZ-Plane XY-Plane

SEM Micrographs of As-built L-PBF Sample

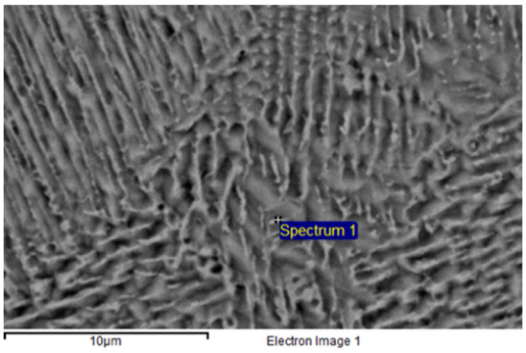

Element	Wt.%	At. %
Cr L	20.86	25.16
Fe L	2.86	3.21
Ni L	51.67	55.21
Nb L	15.35	10.36
Mo L	9.26	6.05
Totals	100.00	

EDS Analysis of L-PBF Sample in As-built Condition

Figure 1. As-built microstructure of LPBF IN625 showing melt pool boundaries, columnar grain growth along the build direction, and a fine cellular substructure associated with rapid solidification.

The combined presence of columnar grain morphology, cellular substructure, and chemical segregation reflects the rapid thermal cycles and limited diffusion associated with LPBF processing. The restricted time available for solute redistribution prevents homogenization, thereby preserving the micro-segregated structure in the as-built condition. These features collectively contribute to the anisotropic behavior commonly reported for LPBF-fabricated IN625.

Overall, the as-built microstructure provides a baseline for evaluating the effectiveness of subsequent heat-treatment processes aimed at reducing segregation, promoting recrystallization, and improving mechanical isotropy.

3.2. Microstructure After Heat Treatment

Application of post-processing heat treatments resulted in substantial modification of the as-built microstructure, with the extent of transformation strongly dependent on the specific thermal route employed. Representative microstructures for the different conditions are shown in Figures 2–4, highlighting the evolution from a highly directional, segregated structure to a more homogeneous, recrystallized morphology.

Under the HT1 condition, which involves high-temperature exposure without pressure assistance, the microstructure exhibits clear evidence of recrystallization. The previously elongated grains are replaced by equiaxed grains containing a high density of annealing twins, indicating that grain boundary migration has occurred during thermal exposure. Despite this transformation, residual heterogeneity remains, suggesting that diffusion was sufficient to initiate recrystallization but not to eliminate compositional gradients fully.

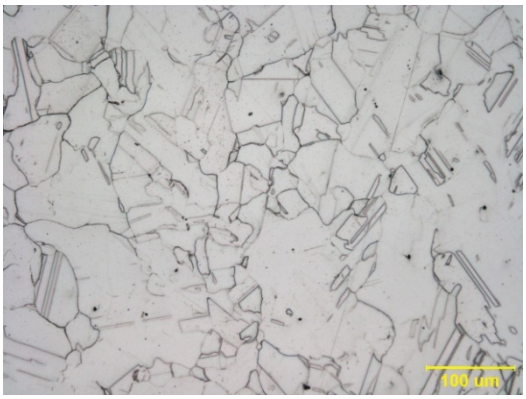

XZ-Plane

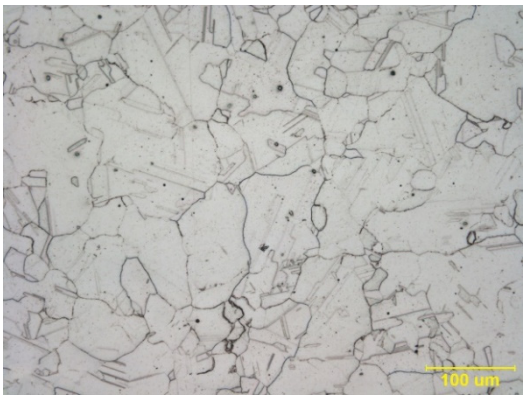

XY-Plane

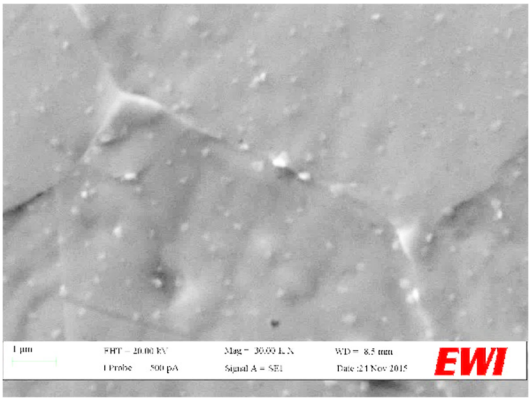

Element	Weight%	Atomic%
C K	24.06	64.64
Ti K	0.68	0.46
Cr K	10.87	6.75
Fe K	1.51	0.87
Ni K	26.90	14.79
Nb L	35.99	12.50

Precipitates at the grain boundary

Figure 2. Microstructure of LPBF IN625 after HT1 treatment showing recrystallized equiaxed grains with annealing twins and Nb-rich carbide precipitates identified by EDS analysis.

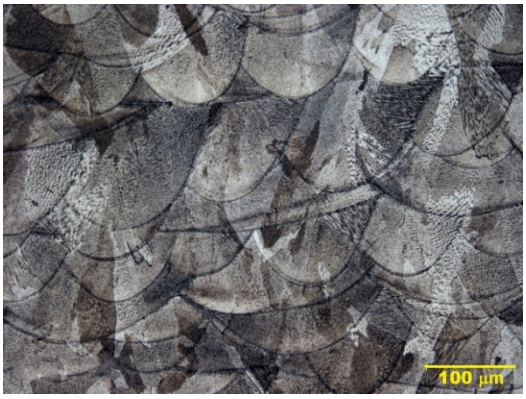

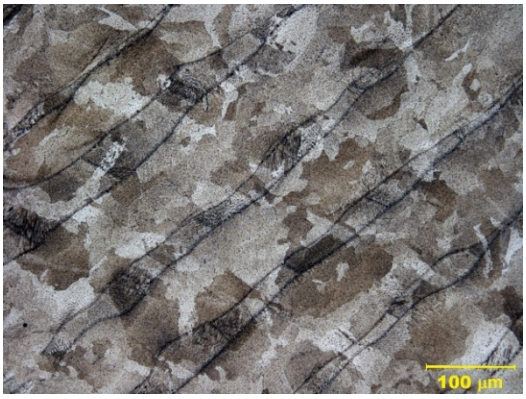

(HT2)

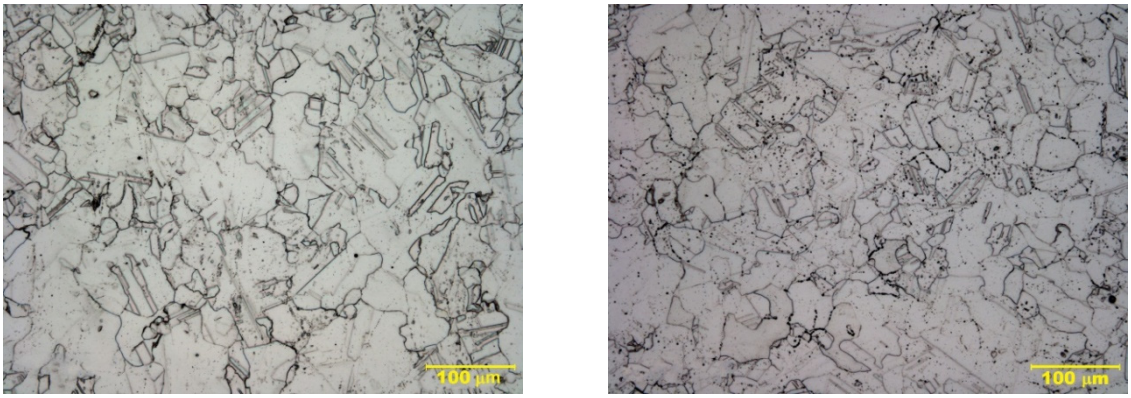

(HT3)

XZ-Plane XY-Plane

Figure 3. Comparison of microstructures for HT2 and HT3 conditions in LPBF IN625, illustrating retention of directional grain morphology after HIP-only processing and formation of a recrystallized equiaxed grain structure following combined thermal and HIP treatment.

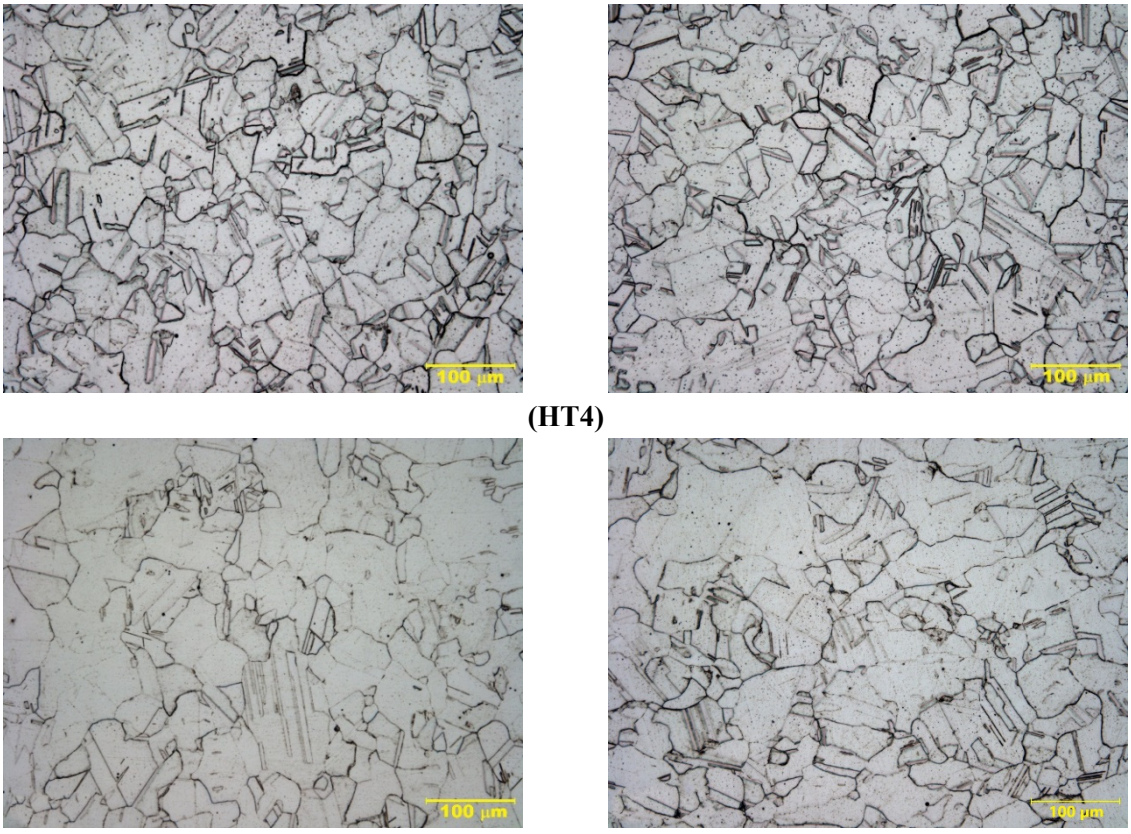

(HT4)

(HT5)

XZ-Plane XY-Plane

Figure 4. Optical microstructures of LPBF IN625 following HT4 and HT5 heat-treatment conditions, showing recrystallized grain structures with variations in grain size and annealing twin density resulting from different thermal exposures.

The HT2 condition, consisting of HIP processing without prior high-temperature stress relief, shows comparatively limited microstructural change. Although porosity reduction is expected under these conditions, the grain structure retains much of the columnar morphology observed in the as-built state. This indicates that the applied thermal cycle during HIP alone does not provide sufficient driving force for the

nucleation and growth of new grains, and that the stored strain energy from the as-built condition is not fully released in the absence of prior thermal exposure.

In contrast, the HT3 condition, which combines stress relief followed by HIP, produces a fully recrystallized microstructure characterized by equiaxed grains with a relatively uniform size distribution. The elimination of the columnar grain structure indicates that the sequential application of thermal exposure and pressure-assisted processing enhances diffusion and facilitates complete recrystallization. This condition also results in a more homogeneous distribution of alloying elements, reflecting a significant reduction of microsegregation.

Microstructural observations further reveal the presence of discrete precipitates following heat treatment. Energy-dispersive spectroscopy (EDS) analysis of these features indicates enrichment in niobium and carbon, consistent with the formation of NbC-type carbides. The absence of significant molybdenum enrichment distinguishes these particles from the Laves phase, which typically exhibits combined Nb–Mo enrichment. This distinction is important, as NbC carbides are thermodynamically stable and contribute to grain boundary strengthening, whereas the Laves phase is generally associated with embrittlement. The observed transition from interdendritic Laves phase in the as-built condition to more stable carbide precipitation after heat treatment reflects the influence of diffusion-driven redistribution of alloying elements.

The HT4 and HT5 conditions, which incorporate higher-temperature solution annealing steps, also produce recrystallized grain structures; however, differences in grain size and twin density are evident. The increased thermal exposure promotes grain growth, resulting in coarser microstructures than HT3. While these conditions further reduce segregation, excessive grain coarsening may compromise mechanical properties by diminishing grain-boundary strengthening.

The observed microstructural evolution can be interpreted in terms of thermally activated diffusion and recrystallization kinetics. Initial heat treatment reduces residual stresses and enables atomic mobility, while subsequent high-temperature exposure facilitates dissolution of segregated phases and promotes grain boundary migration. The addition of HIP enhances densification and accelerates homogenization by increasing the driving force for diffusion. As a result, combined processing routes such as HT3 are more effective in transforming the as-built microstructure into a uniform, isotropic condition.

Overall, the results demonstrate that the sequence and combination of thermal treatments play a critical role in controlling grain morphology, phase distribution, and chemical homogeneity. Among the investigated conditions, HT3 provides the most balanced microstructural refinement, effectively eliminating directional features while avoiding excessive grain growth.

3.3. Grain Size Measurement

Quantitative assessment of grain size was conducted to evaluate the extent of microstructural transformation induced by the different heat-treatment conditions. Measurements were performed on sections extracted in both the build direction (XZ plane) and the transverse direction (XY plane) to capture potential orientation-dependent variations resulting from the LPBF process.

Grain size determination was carried out using the linear intercept approach in accordance with ASTM E112 [53]. Multiple regions within each sample were analyzed to ensure representative sampling, and intercept counts were obtained over several fields of view. The calculated values were averaged to determine the mean grain size for each condition, and statistical variability was assessed from repeated measurements.

The precision of the measurements was quantified using percent relative accuracy (%RA), calculated from the 95% confidence interval relative to the mean grain size. The %RA values ranged from approximately 2.7% to 3.2%, indicating high measurement reliability. These values fall well within the acceptable limits defined by ASTM E112, confirming that the reported grain sizes are statistically meaningful.

The results, summarized in Table 3, show that the as-built condition is characterized by a highly anisotropic grain structure, with elongated grains aligned along the build direction and relatively finer

features in the transverse plane. Following heat treatment, substantial changes in both grain morphology and size are observed, depending on the processing route used.

Among the evaluated conditions, HT3 produces the most uniform grain structure, corresponding approximately to ASTM grain size number G6 in both orientations. The similarity in grain size between the XZ and XY planes indicates that the recrystallization process effectively eliminates the directional grain morphology established during LPBF processing. In contrast, the HT2 condition shows only limited modification relative to the as-built state, confirming that HIP alone does not significantly alter grain structure in the absence of prior thermal activation.

The HT4 and HT5 conditions, which involve higher-temperature exposure, result in coarser grain structures due to enhanced grain growth. While these conditions further reduce microsegregation, the increase in grain size reflects the balance between recrystallization and subsequent grain coarsening under prolonged thermal exposure.

The influence of grain size on mechanical behavior can be interpreted in terms of dislocation–grain boundary interactions. A finer and more uniform grain structure increases the density of grain boundaries, which act as barriers to dislocation motion, thereby enhancing strength while maintaining ductility. The HT3 condition, which yields a refined, isotropic grain structure, therefore provides a favorable combination of mechanical properties, as observed in subsequent tensile testing.

In addition, the reduced variation in grain size across different orientations in the HT3 condition further supports the conclusion that the applied heat-treatment sequence effectively minimizes microstructural anisotropy. This uniformity contributes to the consistent mechanical response observed in both build and transverse directions.

Table 3. Grain size values for LPBF IN625 under different heat-treatment conditions, reported for build (XZ) and transverse (XY) orientations, illustrating the influence of processing route on grain refinement, uniformity, and anisotropy reduction.

Orientation	XZ-Plane	XY-Plane
HT1	4.5	5.0
HT3	6.0	6.0
HT4	4.0	4.5
HT5	4.5	5.0

3.4. Room Temperature Tensile Test

The tensile response of specimens processed under the HT3 condition at ambient temperature is summarized in Figure 5. The reported values correspond to the average of four independent tests for each orientation, and the associated standard deviation remained below ±5% for all measured properties, indicating high repeatability.

At room temperature, the material exhibits an ultimate tensile strength of approximately 880 MPa and a yield strength of approximately 390 MPa. These values exceed the minimum requirements typically specified for additively manufactured IN625 and approach those of conventionally processed material. In addition to strength, the elongation to failure exceeds 50%, indicating substantial ductility.

A key observation is the negligible difference in tensile properties between specimens extracted along the build direction (XZ) and those extracted along the transverse direction (XY). This uniformity in mechanical response indicates that the HT3 heat-treatment sequence effectively mitigates the anisotropy associated with the as-built condition. The elimination of directional grain morphology and reduction of microsegregation contribute to this behavior.

The combination of high strength and ductility can be attributed to the refined, homogeneous microstructure formed during post-processing. The presence of equiaxed grains increases the resistance to

localized deformation, while the reduction of segregated phases minimizes potential sites for crack initiation. As a result, the material exhibits a balanced mechanical response suitable for structural applications.

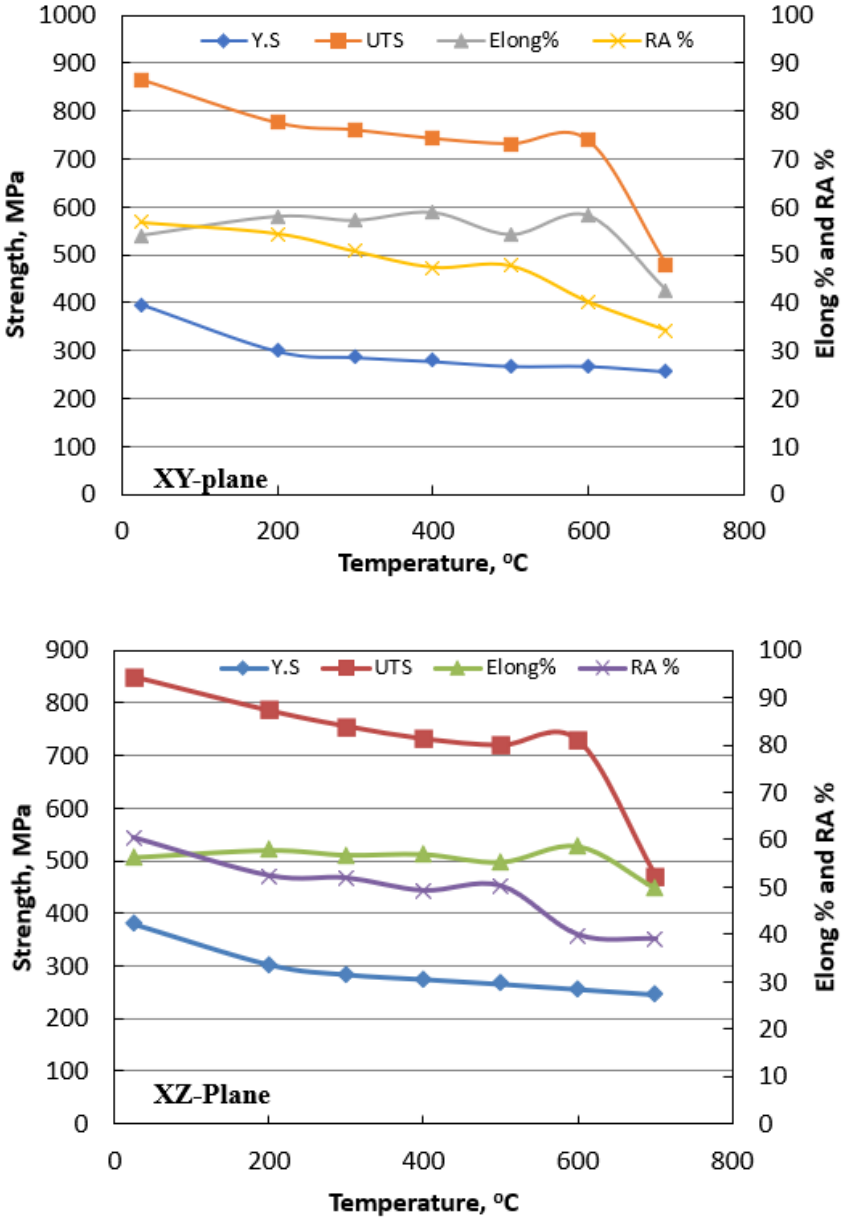

Figure 5. Variation of yield strength, ultimate tensile strength, and elongation with temperature for HT3-treated LPBF IN625, demonstrating mechanical behavior from room temperature to 700 °C in both orientations.

3.5. Elevated Temperature Tensile Test

The tensile behavior at 540 °C was evaluated, with the results also presented in Figure 5. As with the room-temperature measurements, the reported values represent the mean of four specimens, with standard deviation values below ±5%, confirming consistency in the measured response.

At this temperature, the ultimate tensile strength decreases to approximately 735 MPa, while the yield strength is reduced to approximately 270 MPa. This reduction in strength relative to room temperature is consistent with thermally activated deformation mechanisms, where increased atomic mobility facilitates dislocation motion.

Despite the decrease in strength, the elongation remains high, approaching 55%, indicating that the material retains significant ductility at elevated temperatures. The similarity in mechanical behavior

between the XZ and XY orientations persists under these conditions, further confirming that the isotropic microstructure produced by the HT3 treatment is stable at elevated temperatures.

The retention of ductility is associated with the absence of brittle secondary phases and the presence of a uniform grain structure. The recrystallized microstructure promotes homogeneous deformation, while the reduced chemical segregation minimizes localized stress concentrations under load.

3.6. Elevated-Temperature Tensile Curve Between Room Temperature and 700 °C

The variation in mechanical properties as a function of temperature is illustrated in Figure 5, which consolidates tensile results obtained from room temperature up to 700 °C. Across this range, both yield strength and ultimate tensile strength show a gradual decline with increasing temperature, reflecting the reduced resistance to plastic deformation under thermally activated conditions.

An exception to this trend is observed near 600 °C, where a localized increase in strength is evident. This behavior is attributed to dynamic strain aging, a phenomenon associated with interactions between diffusing solute atoms and mobile dislocations. These interactions temporarily restrict dislocation movement, leading to an increase in flow stress within a specific temperature range.

At temperatures above this regime, strength decreases more rapidly as thermal softening becomes dominant. In contrast, elongation generally increases with temperature, indicating enhanced ductility due to increased dislocation mobility. A slight reduction in elongation is observed within the temperature range associated with dynamic strain aging, consistent with localized strain-hardening effects.

Importantly, the mechanical response remains nearly identical in both build and transverse orientations across the entire temperature range. This behavior confirms that the microstructural uniformity achieved through the HT3 processing route is maintained under varying thermal conditions. The combination of stable strength, high ductility, and minimal anisotropy demonstrates the effectiveness of the selected post-processing strategy in producing a reliable and performance-consistent material.

4. Conclusions

The present work examined the influence of multiple post-processing heat-treatment routes on the microstructural development and mechanical behavior of LPBF-fabricated Inconel 625. The results demonstrate that the selection and sequence of thermal treatments play a decisive role in modifying the as-built microstructure and determining the resulting mechanical response.

In the as-built condition, the material exhibits a highly directional grain structure, a cellular substructure, and significant elemental segregation. The enrichment of niobium in interdendritic regions promotes the formation of Nb-rich phases, which are associated with reduced ductility and contribute to anisotropic mechanical behavior.

Application of post-processing treatments leads to substantial microstructural transformation. Among the investigated conditions, the combined stress-relief and HIP sequence (HT3) is the most effective in promoting recrystallization, resulting in a uniform equiaxed grain structure and a significant reduction in compositional heterogeneity. This condition also facilitates the transformation of Nb-rich segregated phases into more stable carbide precipitates, thereby improving microstructural stability.

Grain size measurements confirm that the HT3 condition yields a refined, orientation-independent grain structure, indicating that the directional characteristics introduced during LPBF processing are effectively eliminated. In contrast, treatments involving HIP alone show limited influence on grain morphology, highlighting the importance of prior thermal activation in enabling recrystallization.

Mechanical testing demonstrates that the microstructural refinement achieved under the HT3 condition leads to a favorable combination of strength and ductility. The material exhibits high tensile strength at room temperature and substantial elongation, while maintaining consistent behavior in both build and

transverse orientations. At elevated temperatures, strength decreases as expected; however, the material retains significant ductility and exhibits stable performance over the temperature range investigated.

The temperature-dependent response exhibits a localized increase in strength near intermediate temperatures, attributed to dynamic strain aging arising from interactions between solute atoms and dislocations. Despite this effect, the overall mechanical behavior remains consistent and predictable.

Collectively, the results indicate that appropriately designed post-processing strategies can effectively transform the LPBF-induced microstructure into a homogeneous, isotropic state. The HT3 processing route, in particular, provides an optimal balance between recrystallization, phase stability, and mechanical performance, making it a suitable approach for applications requiring reliable structural behavior over a wide range of service temperatures.

Statement of the Use of Generative AI and AI-Assisted Technologies in the Writing Process

During the preparation of this work, the authors used Grammarly Pro in order to improve readability and language. After using this tool/service, the author reviewed and edited the content as needed and took full responsibility for the publication's content.

Acknowledgments

The author would like to acknowledge the Additive Manufacturing team at Edison Welding Institute (EWI) for their valuable contributions to this work. Their support in specimen fabrication, process execution, and technical discussions was essential to the successful completion of this study

Ethics Statement

Not applicable.

Informed Consent Statement

Not applicable.

Data Availability Statement

The data that support the findings of this study are available from the corresponding author upon reasonable request. Certain data may be subject to confidentiality or proprietary restrictions due to the nature of the research and associated project agreements.

Funding

This research received no external funding.

Declaration of Competing Interest

The authors declare that they have no known competing financial interests or personal relationships that could have appeared to influence the work reported in this paper.

References

1. Zhang D, Feng Z, Wang C, Wang W, Liu Z, Niu W. Comparison of microstructures and mechanical properties of Inconel 718 alloy processed by selective laser melting and casting. *Mater. Sci. Eng. A* **2018**, *724*, 357–367. DOI:10.1016/j.msea.2018.03.073
2. Chlebus E, Gruber K, Kuznicka B, Kurzac J, Kurzynowski T. Effect of heat treatment on the microstructure and mechanical properties of Inconel 718 processed by selective laser melting. *Mater. Sci. Eng. A* **2015**, *639*, 647–655. DOI:10.1016/j.msea.2015.05.035

3. Zhang D, Niu W, Cao X, Liu Z. Effect of standard heat treatment on the microstructure and mechanical properties of selective laser melting manufactured Inconel 718 superalloy. *Mater. Sci. Eng. A* **2015**, *644*, 32–40. DOI:10.1016/j.msea.2015.06.021
4. Popovich VA, Borisov EV, Popovich AA, Sufiiarov VS, Masaylo DV, Alzina L. Impact of heat treatment on the mechanical behavior of Inconel 718 processed with tailored microstructure by selective laser melting. *Mater. Des.* **2017**, *131*, 12–22. DOI:10.1016/j.matdes.2017.05.065
5. Barros R, Silva FJG, Gouveia RM, Saboori A, Marchese G, Biamino S, et al. Laser powder bed fusion of Inconel 718: Residual stress analysis before and after heat treatment. *Metals* **2019**, *9*, 1290. DOI:10.3390/met9121290
6. Zhang YC, Jiang W, Tu ST, Zhang XC, Ye YJ, Wang RZ. Experimental Investigation and Numerical Prediction on Creep Crack Growth Behaviour of the Solution Treated Inconel 625 Superalloy. *Eng. Fract. Mech.* **2018**, *199*, 327–342. DOI:10.1016/j.engfracmech.2018.05.048
7. Xu X, Mi G, Xiong L, Jiang P, Shao X, Wang C. Morphologies, Microstructures and Properties of TiC Particle Reinforced Inconel 625 Coatings Obtained by Laser Cladding with Wire. *J. Alloys Compd.* **2018**, *740*, 16–27. DOI:10.1016/j.jallcom.2017.12.298
8. Cinoglu IS, Charbal A, Vermaak N. Towards Exploiting Inelastic Design for Inconel 625 under Short-Term Cyclic Loading at 600 °C. *Mech. Mater.* **2020**, *140*, 103219. DOI:10.1016/j.mechmat.2019.103219
9. Huebner J, Kata D, Kusiński J, Rutkowski P, Lis J. Microstructure of Laser Cladded Carbide Reinforced Inconel 625 Alloy for Turbine Blade Application. *Ceram. Int.* **2017**, *43*, 8677–8684. DOI:10.1016/j.ceramint.2017.03.194
10. Zhang HY, Zhang SH, Cheng M, Li ZX. Deformation characteristics of δ phase in the delta-processed Inconel 718 alloy. *Mater. Charact.* **2010**, *61*, 49–53. DOI:10.1016/j.matchar.2009.10.003
11. Liu FC, Lin X, Yang GL, Song MH, Chen J, Huang W. Microstructure and residual stress of laser rapid formed Inconel 718 nickel-base superalloy. *Opt. Laser Technol.* **2011**, *43*, 208–213. DOI:10.1016/j.optlastec.2010.06.015
12. Rai SK, Kumar A, Shankar V, Jayakumar T, Rao KBS, Raj B. Characterization of Microstructures in Inconel 625 using X-ray Diffraction Peak Broadening and Lattice Parameter Measurements. *Scripta Mater.* **2004**, *51*, 59–63. DOI:10.1016/j.scriptamat.2004.03.017
13. Evans ND, Maziasz PJ, Shingledecker JP, Yamamoto Y. Microstructure Evolution of Alloy 625 Foil and Sheet during Creep at 750 °C. *Mater. Sci. Eng. A* **2008**, *498*, 412–420. DOI:10.1016/j.msea.2008.08.017
14. Rodriguez R, Hayes RW, Berbon PB, Lavernia EJ. Tensile and Creep Behaviour of Cryomilled Inco 625. *Acta Mater.* **2003**, *51*, 911–929. DOI:10.1016/S1359-6454(02)00494-9
15. Mathew MD, Rao KBS, Mannan SL. Creep Properties of Service-Exposed Alloy 625 after Re-solution Annealing Treatment. *Mater. Sci. Eng. A* **2004**, *372*, 327–333. DOI:10.1016/j.msea.2004.01.042
16. Bean E, McLouth TD, Witkin DB, Sitzman SD, Adams PM, Zaldivar PMRJ. Build orientation effects on texture and mechanical properties of selective laser melting Inconel 718. *J. Mater. Eng. Perform.* **2019**, *28*, 1942–1949. DOI:10.1007/s11665-019-03980-w
17. Cabrini M, Lorenzi S, Testa C, Brevi F, Biamino S, Fino P, et al. Microstructure and Selective Corrosion of Alloy 625 Obtained by Means of Laser Powder Bed Fusion. *Materials* **2019**, *12*, 1742. DOI:10.3390/ma12111742
18. Shi R, Khairallah SA, Roehling TT, Heo TW, McKeown JT, Matthews MJ. Microstructural control in metal laser powder bed fusion additive manufacturing using laser beam shaping strategy. *Acta Mater.* **2020**, *184*, 284–305. DOI:10.1016/j.actamat.2019.11.053
19. Raghavan N, Simunovic S, Dehoff R, Plotkowski A, Turner J, Kirka M, et al. Localized melt-scan strategy for site-specific control of grain size and primary dendrite arm spacing in electron beam additive manufacturing. *Acta Mater.* **2017**, *140*, 375–387. DOI:10.1016/j.actamat.2017.08.038
20. Roehling TT, Wu SSQ, Khairallah SA, Roehling JD, Soezeri SS, Crumb MF, et al. Modulating laser intensity profile ellipticity for microstructural control during metal additive manufacturing. *Acta Mater.* **2017**, *128*, 197–206. DOI:10.1016/j.actamat.2017.02.025
21. Luna V, Trujillo L, Gamon A, Arrieta E, Murr LE, Wicker RB, et al. Comprehensive and comparative heat treatment of additively manufactured Inconel 625 alloy and corresponding microstructures and mechanical properties. *Manuf. Mater. Process.* **2022**, *6*, 107–124. DOI:10.3390/jmmp6050107
22. Gamon A, Arrieta E, Gradl PR, Katsarelis C, Murr LE, Wicker RB, et al. Microstructure and hardness comparison of as-built Inconel 625 alloy following various additive manufacturing processes. *Results Mater.* **2021**, *12*, 100239. DOI:10.1016/j.rinma.2021.100239
23. Vilaro T, Colin C, Bartout JD, Nazé L, Sennour M. Microstructural and mechanical approaches of the selective laser melting process applied to a nickel-base superalloy. *Mater. Sci. Eng. A* **2012**, *534*, 446–451. DOI:10.1016/j.msea.2011.11.092

24. *AMS666K*; Nickel Alloy, Corrosion and Heat-Resistant, Bars, Forgings, Extrusions, and Rings 62Ni–21.5Cr–9.0Mo–3.65 (Cb [Nb]+Ta) Annealed. SAE International: Warrendale, PA, USA, 2022.
25. *AMS5599J*; Nickel Alloy, Corrosion and Heat-Resistant, Sheet, Strip, and Plate 62Ni–21.5Cr–9.0Mo–3.7 Cb (Nb) Solution Heat Treated. SAE International: Warrendale, PA, USA, 2022.
26. Leary M. *Chapter 11—Powder Bed Fusion*; Elsevier: Amsterdam, The Netherlands, 2020. DOI:10.1016/B978-0-12-816721-2.00011-7
27. Fang ZC, Wu ZL, Huang CG, Wu CW. Review on residual stress in selective laser melting additive manufacturing of alloy parts. *Opt. Laser Technol.* **2020**, *129*, 106283. DOI:10.1016/j.optlastec.2020.106283
28. Blakey-Milner B, Gradl P, Snedden G, Brooks M, Pitot J, Lopez E, et al. Metal additive manufacturing in aerospace—A review. *Mater. Des.* **2021**, *209*, 110008. DOI:10.1016/j.matdes.2021.110008
29. Marchese G, Lorusso M, Parizia S, Bassini E, Lee J, Calignano F, et al. Influence of heat treatments on microstructure evolution and mechanical properties of Inconel 625 processed by laser powder bed fusion. *Mater. Sci. Eng. A* **2018**, *729*, 64–75. DOI:10.1016/j.msea.2018.05.044
30. Li C, White R, Fang XY, Weaver M, Guo YB. Microstructure evolution characteristics of Inconel 625 alloy from selective laser melting to heat treatment. *Mater. Sci. Eng. A* **2017**, *705*, 20–31. DOI:10.1016/j.msea.2017.08.058
31. Roy TD, Wei HL, Zuback JS, Mukherjee T, Elmer JW, Milewski JO, et al. Additive manufacturing of metallic components—Process, structure and properties. *Prog. Mater. Sci.* **2018**, *92*, 112–224. DOI:10.1016/j.pmatsci.2017.10.001
32. *ASTM F3056*; Standard Specification for Additive Manufacturing Nickel Alloy (UNS N06625) with Powder Bed Fusion. ASTM International: West Conshohocken, PA, USA, 2014.
33. Liu J, Yang HY, Zhong XM, Dong BY, Li ZY, Chen JB, et al. Microstructure manipulation and high-temperature service performance enhancement of nickel-based superalloys, *J. Mater. Res. Tech*. **2026**, *40*, 2930–2961. DOI:10.1016/j.jmrt.2025.12.205
34. Degnah A, Tabbakh T, Kurdi A, Basak AK. Role of precipitation and solute segregation on micro-scale deformation of additively manufactured Inconel 718. *Mater. Sci. Eng. A* **2023**, *887*, 145762. DOI:10.1016/j.msea.2023.145762
35. Devaux A, Naze L, Molins R, Pineau A, Organista A, Guedou JY, et al. Gamma double prime precipitation kinetic in Alloy 718. *Mater. Sci. Eng.* **2008**, *486*, 117–122. DOI:10.1016/j.msea.2007.08.046
36. Smith GD, Patel SJ. *The Role of Niobium in Wrought Precipitation Hardened Nickel Base Alloys*; Sixth International Symposium on Superalloys 718, 625, 706 and Derivatives 2005; Loria EA, Ed.; TMS (The Minerals, Metals & Materials Society): Pittsburgh, PA, USA, 2005; pp. 135–154.
37. Kreitcberg A, Brailovski V, Turenne S. Effect of heat treatment and hot isostatic pressing on the microstructure and mechanical properties of Inconel 625 alloy processed by laser powder bed fusion. *Mater. Sci. Eng. A* **2017**, *689*, 1–10. DOI:10.1016/j.msea.2017.02.038
38. Murr LE, Martinez E, Gaytan SM, Ramirez DA, Machado BI, Shindo PW, et al. Microstructural architecture, microstructures, and mechanical properties for a Nickel-Base Superalloy fabricated by Electron Beam Melting. *Metall. Mater. Trans. A* **2011**, *42*, 3491–3508. DOI:10.1007/s11661-011-0748-2
39. Kreitcberg A, Brailovski V, Turenne S. Elevated temperature mechanical behavior of IN625 alloy processed by laser powder-bed fusion. *Mater. Sci. Eng. A* **2017**, *700*, 540–553. DOI:10.1016/j.msea.2017.06.045
40. Hrutkay K, Kaoumi D. Tensile deformation behavior of a nickel-based superalloy at different temperatures. *Mater. Sci. Eng. A* **2014**, *599*, 196–203. DOI:10.1016/j.msea.2014.01.056
41. Hale C, Rollings W, Weaver M. Activation energy calculations for discontinuous yielding in Inconel 718SPF. *Mater. Sci. Eng. A* **2001**, *300*, 153–164. DOI:10.1016/S0921-5093(00)01470-2
42. Rahman MS, Priyadarshan G, Raja KS, Nesbitt C, Misra M. Characterization of high-temperature deformation behavior of IN 617. *Mech. Mater.* **2009**, *41*, 261–270. DOI:10.1016/j.mechmat.2008.10.003
43. Wright JK, Carroll LJ, Cabet C, Lillo TM, Benz JK, Simpson JA, et al. Characterization of elevated temperature properties of heat exchanger and steam generator alloys. *Nucl. Eng.* **2012**, *251*, 252–260. DOI:10.1016/j.nucengdes.2011.10.034
44. Fournier L, Delafosse D, Magnin T. Oxidation induced intergranular cracking and Portevin-Le Chatelier effect in nickel-base superalloy 718. *Mater. Sci. Eng. A* **2001**, *316*, 166–173. DOI:10.1016/S0921-5093(01)01224-2
45. Kaoumi D, Hrutkay K. Tensile deformation behavior and microstructure evolution of Ni-based superalloy 617. *J. Nucl. Mater.* **2014**, *454*, 265–273. DOI:10.1016/j.jnucmat.2014.08.003
46. Mo K, Lovicu G, Chen X, Tung HM, Hansen JB, Stubbins JF. Mechanism of plastic deformation of a Ni-based superalloy for VHTR applications. *J. Nucl. Mater.* **2013**, *441*, 695–703. DOI:10.1016/j.jnucmat.2013.03.083
47. Nalawade SA, Sundararaman M, Kishore R, Shah JG. The influence of ageing on the serrated yielding phenomenon in a nickel-base superalloy. *Scr. Mater.* **2008**, *59*, 991–994. DOI:10.1016/j.scriptamat.2008.07.004

48. Amato KN, Hernandez J, Murr LE, Martinez E, Gaytan SM, Shindo PW. Microstructures and mechanical behavior of Inconel 625 fabricated by selective laser melting. *Acta Mater.* **2012**, *60*, 2229–2239. DOI:10.1016/j.actamat.2011.12.032
49. Kuo YC, Kakehi K. Effects of heat treatment on microstructure and mechanical properties of selective laser melted Inconel 625 alloy. *J. Alloys Compd.* **2020**, *815*, 152404. DOI:10.1016/j.jallcom.2019.152404
50. Zhihua T, Chaoqun Z, Dayong W, Daniel W, Yongtao Z, Yingtao T. A Review on laser powder bed fusion of Inconel 625 nickel-based alloy. *Appl. Sci*. **2020**, *10*, 81–95. DOI:10.3390/app10010081
51. Jie Z, Kai F, Hiroyuki K, Zhuguo L. Effect of heat treatment on the anisotropic mechanical properties and corrosion resistance of laser powder bed fusion fabricated Inconel 625. *J. Alloys Compd.* **2024**, *1001*, 175087. DOI:10.1016/j.jallcom.2024.175087
52. Ma K, Wang J. Microstructural Characteristics and Mechanical Properties of an Additively Manufactured Nickel-Based Superalloy. *Crystals* **2022**, *12*, 1358. DOI:10.3390/cryst12101358
53. *ASTM E112-13*; Standard Test Methods for Determining Average Grain Size. ASTM International: West Conshohocken, PA, USA, 2025.
54. *ASTM E8/E8M-21*; Standard Test Methods for Tension Testing of Metallic Materials. ASTM International: West Conshohocken, PA, USA, 2021.
55. *ASTM E21-20*; Standard Test Methods for Elevated Temperature Tension Tests of Metallic Materials. ASTM International: West Conshohocken, PA, USA, 2020.